Formation, structure, and bonding of boron-vacancy pairs in graphene: A first-principles study

Kyoung Eun Kweon[1] and Gyeong S. Hwang[2,*]
[1]*Department of Electrical and Computer Engineering, The University of Texas, Austin, Texas 78712, USA*
[2]*Department of Chemical Engineering, The University of Texas, Austin, Texas 78712, USA*
(Received 18 September 2010; published 22 November 2010)

Using density-functional theory calculations, we examine how a mobile single vacancy (V) interacts with substitutional boron (B) in graphene and the effect of boron-vacancy (BV) pairing on the electronic structure of graphene. We find that B in a BV pair energetically favors fourfold coordination, rather than remaining twofold coordinated, by forming a distorted tetrahedral structure with neighboring C lattice atoms. In the fourfold state, the binding energy of a BV pair is predicted to be 2.54 eV with respect to B and V. Our calculations also suggest magnetic-moment oscillations by interconversion between the twofold (1 μ_B) and fourfold (0 μ_B) states, as their energy difference is rather moderate ($\approx$0.3 eV). We also discuss the bonding mechanisms of a BV pair in the twofold and fourfold states and modifications in the electronic structure of graphene by BV pairing as compared to isolated B and V cases. Finally, the pathways and energetics of V migration in the vicinity of B are calculated; the results suggest that B is likely to trap mobile single vacancies within a certain radius and can possibly serve as an anchor for vacancy clusters.

DOI: 10.1103/PhysRevB.82.195439 PACS number(s): 81.05.ue, 61.48.Gh, 73.22.Pr

I. INTRODUCTION

Graphene, a honeycomb-shaped single layer of graphite, has been of great recent interest in science and engineering due to its unique chemical and physical properties. Graphene, carbon nanotubes, and other graphitic carbon nanostructures have been extensively researched for their potential applications in electronics, photonics, hydrogen storage, sensing, and batteries.[1–9] Of particular importance is to understand how to tune the electronic structure of graphene-based materials through introduction of chemical impurities and/or creation of defects, to obtain their desired physical and chemical properties for any targeted applications.

Boron is one of the most important substitutional dopants for carbon-based materials because of its comparable atomic size with carbon. Boron has one less valence electron than carbon, which can allow for a substantial modification of the electronic and magnetic properties of graphitic systems.[4,10] Substitutional B in graphene has been experimentally observed through techniques such as x-ray adsorption spectroscopy and high-resolution scanning tunneling microscopy (STM).[11,12] The presence of B in carbon nanostructures allows the selective sensing of harmful NO and NO_2 gases, better Li storage as a battery anode, and enhanced H storage.[2–8] The effects of B incorporation have also been studied for potential electronics applications.[13] In addition, graphene often consists of a large number of vacancy defects that can modify the electronic structure to a large extent; for instance, they are known to induce magnetism in otherwise nonmagnetic graphene.[14–16] Vacancies have been observed and characterized using advanced microscopy techniques such as transmission electron microscopy.[17] It has been shown that single vacancies may undergo migration in graphene with moderate activation energy,[18,19] thereby allowing the vacancy and immobile substitutional dopants to possibly meet. Despite the importance, only a few studies have been performed on the nature and formation of dopant-vacancy complexes in graphene. The structure of some dopant-vacancy pairs has been examined in graphite,[20] however, there is still much to be learned from the study of dopant-defect interactions in graphene.

In this paper, we present the formation, structure, and electronic properties of boron-vacancy complexes in graphene based on spin-polarized density-functional theory (DFT) calculations. First, we look at the atomic and electronic structures of B-doped and undoped graphene sheets, for the sake of reference. Then, we examine possible atomic configurations for a BV pair and how the BV pairing modifies the electronic structure of graphene as compared to substitutional B and single V cases. Finally, we calculate the viable routes and energy barriers of BV pairing (or dissociation) that occurs through V migration. The improved understanding could offer insight into how to tune the properties of graphene by engineering defects and impurities.

II. CALCULATION METHODS

The calculations reported herein were performed on the basis of DFT within the generalized gradient approximation (GGA-PW91),[21] as implemented in the Vienna *ab initio* simulation package (VASP).[22] The projector augmented wave method with a plane-wave basis set was used to describe the interaction between ion cores and valence electrons.[23] We used a 112-atom rectangular graphene sheet with dimensions of 17.0882×17.2654 Å^2; here, the GGA-optimized lattice constant of 2.467 Å was employed, which is slightly larger than the experimental value of 2.461 Å. Periodic boundary conditions were employed in all three directions with a vacuum gap of 10 Å in the vertical (z) direction to separate the system from its periodic images. During geometry optimization (energy minimization), all atoms were fully relaxed using conjugate gradient method until residual forces on constituent atoms become smaller than 3×10^{-2} eV/Å. In geometry optimization, we employed a plane-wave cutoff energy of 408 eV and a $(3 \times 3 \times 1)$ k-point grid in the scheme of Monkhorst-Pack for the Brillouin zone sampling.[24] To ob-

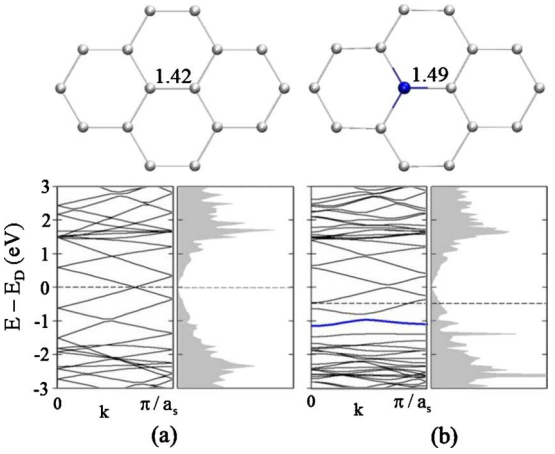

FIG. 1. (Color online) Optimized configurations (upper panels) and corresponding electronic band structure and total DOS (bottom panels) of (a) pristine and (b) 0.9% boron-doped graphene sheets. Grey and black (blue) balls represent C and B atoms, respectively, and the C-C and C-B bond lengths indicated are given in angstrom. In each band structure and DOS plot, the Dirac energy (E_D) is set to 0 eV while the horizontal dotted line indicates the Fermi level position. In (b) the B impurity level is indicated by a thick (blue) solid line.

tain accurate electron density of states (DOS) and charge densities, a gamma-centered $(6\times6\times1)$ k-point mesh was used; the DOS were calculated using the tetrahedron method with Blöchl corrections.[25] The spin interpolation formula proposed by Vosko *et al.*[26] was used to estimate magnetic moments. Reaction pathways and barriers were determined using the climbing-image nudged elastic band method with 6–8 intermediate images for each elementary step.[27]

III. RESULTS AND DISCUSSION

Substitutional boron. For the sake of reference, first we calculated how the atomic and electronic structure of graphene changes when one C is replaced with B. The substitutional B exhibits a planar sp^2-like configuration. As shown in Fig. 1 (upper panels), the B-C bond distance of 1.49 Å [Fig. 1(b)] is greater than the C-C bond distance of 1.42 Å in the pristine graphene [Fig. 1(a)], which is consistent with STM images reported for B-doped graphite.[12] The longer B-C bond is partly attributed to the larger size of B compared to C; note that the atomic radii of B and C are 0.82 Å and 0.77 Å, respectively.[28] Figure 1 (lower panels) shows the electronic structures of B-doped and intrinsic graphene. The B-doped and undoped graphene sheets turn out to have no net magnetic moment. For pristine graphene [Fig. 1(a)], the valence and conduction bands touch and both bands exhibit conical band dispersion near the Dirac point, where the Fermi level is located. For the B-doped case [Fig. 1(b)], the Fermi level shifts down into the valence band due to hole injection into the π-electron system of graphene; as such, the Fermi-level position is a function of B concentration. The B p_z orbital is partially filled by the transferred charge while the B impurity level [thick (blue) solid line in Fig. 1(b)] is located below the Fermi level. Our results are

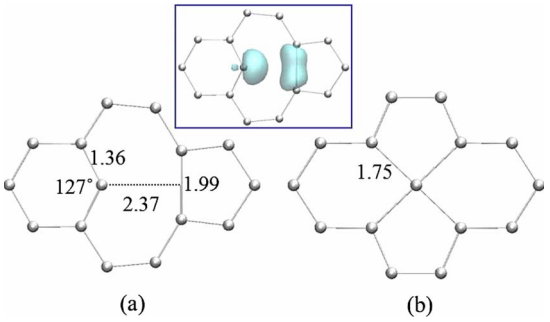

FIG. 2. (Color online) (a) Local minimum and (b) (fourfold-coordinated) local maximum configurations of a single atom vacancy; C-C bond lengths indicated are given in angstrom. In the inset, the unpaired and paired electrons are represented by maximally localized Wannier functions (with an isosurface value of 0.95 electron/Å^3), which were calculated using the CPMD package (Ref. 30).

overall in good agreement with previous theoretical studies of B-doped graphene sheets and nanoribbons.[10,11,29]

Single vacancy. Upon removal of one C atom from an intrinsic graphene sheet, each of the three neighboring atoms has one localized sp^2 dangling bond. As illustrated in Fig. 2(a), the following symmetry-lowering lattice relaxation causes two neighboring atoms to form a weak covalent bond [as demonstrated by Wannier function (WF) analysis, Fig. 2 (inset)]. The remaining unsaturated C atom protrudes out of plane by 0.16 Å, due in part to the repulsion between the unpaired and paired electrons. A single vacancy may undergo migration through the transition state as shown in Fig. 2(b); our calculation predicts the migration barrier to be 1.42 eV, within the range 0.9–1.6 eV of previous calculations.[18–20,31]

As shown in the electron DOS [Fig. 3(a)], the (unpaired) sp^2 dangling bond state is located at 0.4 eV below the Fermi level, and the quasilocalized p_z states caused by the single-atom vacancy appear at the Fermi level. The contour plot in Fig. 3(b) illustrates the difference between the majority (up) and minority (down) spin densities of states as shown in the DOS plot [Fig. 3(a)]. Substantial spin differences occur in the localized sp^2 dangling bond state and quasilocalized p_z states, giving rise to ferromagnetism. The total magnetic moment is predicted to be 1.27 μ_B (for 0.9% vacancy concentration), in good agreement with previous studies[14,15] while the magnetic momentum is likely a function of vacancy concentration. Our calculations also show that the magnetic momentum is sensitive to the weak C-C bond length, although the total-energy variation is insignificant with the bond length. As illustrated in Fig. 3(c), when the sp^2 dangling bond is saturated by a hydrogen atom, the C-C bond distance slightly decreases from 1.99 to 1.91 Å. The dangling bond termination likely leaves all spins paired; according to our calculations, the antiferromagnetic and ferromagnetic ($\approx$0.37 μ_B) states are energetically nearly degenerate.

Boron-vacancy pair. If a mobile vacancy meets with a substitutional B, a BV pair can be formed. As shown in Fig. 4(a) (left panel), when a vacancy is placed adjacent to substitutional B, the distance between two unsaturated C atoms is significantly elongated to 2.58 Å as compared to the vacancy case (1.99 Å). For the BV geometry, the energy gain

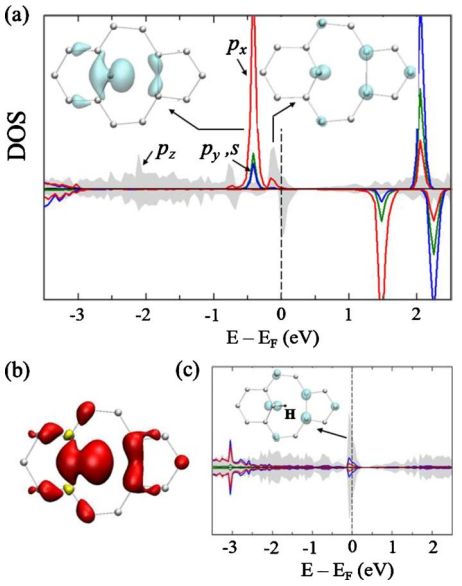

FIG. 3. (Color online) Density of states projected onto the s, p_x, p_y, and p_z states of the three C atoms surrounding the vacancy site; (a) without and (c) with H termination of the unsaturated sp^2 dangling bond. The shaded gray area represents the p_z states, and the red, blue, and green solid lines indicate the p_x, p_y, and s states, respectively. Band-decomposed charge densities near the Fermi level (E_F) are also plotted with an isosurface value of 0.04 electron/Å^3 (based on the total density of states, not shown); (a) -0.50 eV$<E-E_F<-0.30$ eV (mainly corresponding to the sp^2 dangling bond state) and -0.20 eV$<E-E_F<0$ eV (mainly the p_z states due to vacancy creation) and (c) -0.15 eV$<E-E_F<0$ eV. (b) Spin-density difference between the majority (spin up) and minority (spin down) states in (a) $[=\rho(\uparrow)-\rho(\downarrow)]$; the black (red) and gray (yellow) colors indicate the regions with excess majority and minority spin electrons, respectively. The isosurface value is set to 0.02 electron/Å^3.

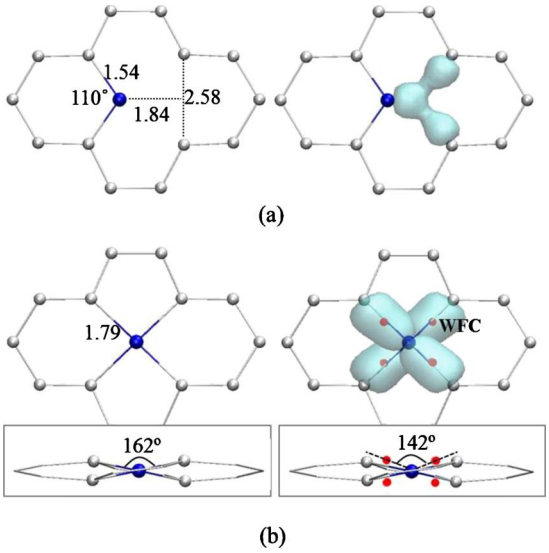

FIG. 4. (Color online) Optimized configurations of a BV pair for (a) twofold B and (b) fourfold B states. Grey and black (blue) balls represent C and B atoms, respectively, and the bond lengths indicated are given in angstrom. The bonding interactions between the B and neighboring C atoms are also represented by maximally localized Wannier functions (with an isosurface value of 0.95 electron/Å^3) (right panels). Insets in (b) show the side views of the fourfold-state configurations; small black (red) balls represent WFCs.

from pairing is predicted to be 2.21 eV with respect to B and single V. The large C-C distance implies that there is no bonding interaction between them; instead, the C atoms interact with the B atom while they all remain in plane, as demonstrated by analysis of WFs [Fig. 4(a) (right panel)]. Looking at the electron DOS in Fig. 5(a), the B sp^2 orbital is fully filled, and it is likely mixed with the partially filled C sp^2 orbitals. The filling of the B sp^2 orbital is somewhat analogous to adduction of an electron-donor molecule (such as carbon monoxide and nitrogen) to the twofold B in a six-membered aromatic ring (such as C_5H_5B, where B is highly unstable due to electron deficiency).[32] The partially saturated sp^2 states of the undercoordinated C atoms are located at the Fermi level, along with the quasilocalized p_z states around the vacancy site, where majority-spin electrons exist in excess as demonstrated by the spin-density difference plot [inset in Fig. 5(a)]. The net magnetic moment is predicted to be about 1.0 μ_B.

Our calculation predicts that the twofold B state may undergo conversion to the more stable fourfold state with a small energy barrier ($\approx$0.06 eV) and a sizable exothermicity ($\approx$0.33 eV) [see Fig. 4(b)]. As stated earlier, for V the fourfold state [Fig. 2(b)] is the saddle point between two adjacent local minima with a saddle-minima energy difference of 1.42 eV. In the fourfold state, the B atom is likely to accept electron, resulting in hole states in graphene [see Fig. 5(b)]. Similar to the $[BH_4]^-$ anion, the fourfold B tends to favor a tetrahedral (sp^3) structure as opposed to square planar;[33] however, due to the rest of the in-plane C lattice, a perfect tetrahedron (having C-B-C angles of 109°) is highly unlikely to form. Instead, the fourfold B adopts a distorted tetrahedral configuration where the neighboring C atoms are displaced by $\pm$0.27 Å perpendicular to the graphene plane, resulting in C-B-C angles of 162° and WF center (WFC)-B-WFC angles of 142°. As shown in LDOS [Fig. 5(b)], the structural distortion leads to a distinct splitting in the B p_x, p_y, and p_z states, instead of sp^3 hybridization as typically seen for a tetrahedron structure. The four B-C bonds are equal in length (1.79 Å) because of resonance, slightly longer than a single B-C bond (1.65 Å). Our calculation shows that the fourfold BV structure is nonmagnetic. This suggests that the interconversion between the twofold and fourfold states, which appears to rather easily occur (with moderate barriers of 0.06/0.39eV) at elevated temperatures, would induce magnetic-moment oscillations (approximately between 1 and 0 μ_B).

B$+V\leftrightarrow$BV. We examined dissociation of a BV pair by the departure of the mobile V from the B site; in the absence of B, the V migration barrier is predicted to be 1.42 eV, as stated earlier. Figure 6 shows variations in the total energy and barrier of V migration in terms of the location of V with respect to B. V migration from site 1 to site 2 ($1\rightarrow2$) is predicted to occur by crossing a barrier of 1.63 eV with a return barrier of 0.56 eV. From site 2, the V can further migrate along two different paths (either to site 3 or 3′) or in

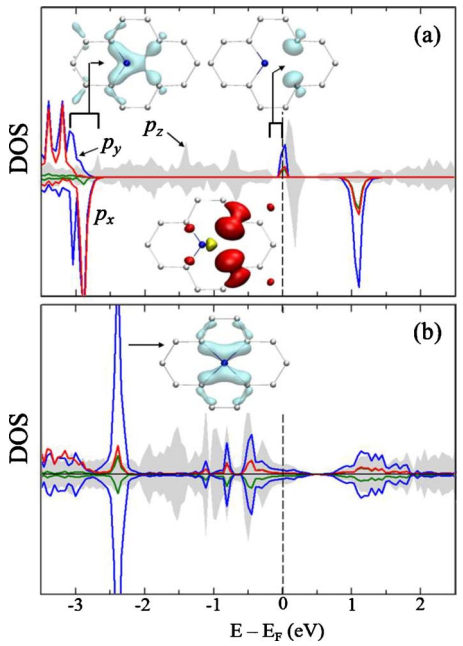

FIG. 5. (Color online) Density of states projected onto the s, p_x, p_y, and p_z states of the B and nearest C atoms for (a) twofold B and (b) fourfold B states. The shaded gray area represents the p_z states, and the red, blue, and green solid lines indicate the p_x, p_y, and s states, respectively. Band-decomposed charge densities for selected states (as indicated) are also plotted with an isosurface value of 0.09 electron/Å^3 (based on the total density of states, not shown). Inset in (a) shows the difference between the majority (up) and minority (down) spin states [$=\rho(\uparrow)-\rho(\downarrow)$] near the Fermi level; the black (red) and gray (yellow) colors indicate the regions with excess majority and minority spin electrons, respectively. The isosurface value is set to 0.03 electron/Å^3.

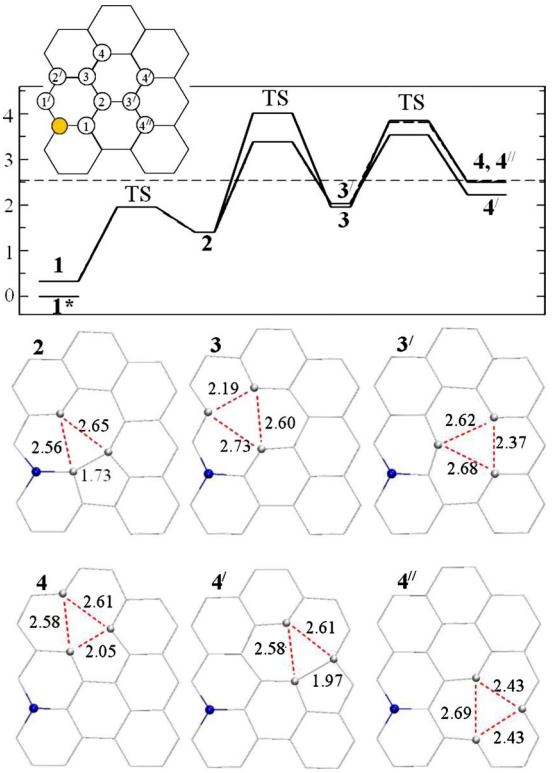

FIG. 6. (Color online) Energy variation (in eV) in terms of vacancy location with respect to B together with corresponding atomic configurations. For the BV pair, 1* refers to the fourfold B state [Fig. 4(b)] while 1 and 1′ represent the twofold state [Fig. 4(a)]. The bond lengths indicated are given in angstrom.

the return direction. Although sites 3 and 3′ are comparable in energy, the barrier for $2\rightarrow3$ (2.63 eV) is 0.64 eV higher than the barrier for $2\rightarrow3'$ (1.99 eV). This can possibly be explained by looking at the associated lattice strain (or strain energy) around B. In the $2\rightarrow3$ and $2\rightarrow3'$ transition states, the average distance between the B atom and the three adjacent C atoms is 1.47 Å for $2\rightarrow3$ and 1.53 Å for $2\rightarrow3'$. When the V is in site 2, the average C-B distance is 1.57 Å, which indicates that the $2\rightarrow3$ transition would require larger (compressive) lattice strain. The resulting larger strain energy might be responsible for the higher energy barrier in the $2\rightarrow3$ migration. From site 3, the V can move to site 4 with a barrier of 1.90 eV or to site 2′ with a barrier of 2.07 eV (note that the transition $3\rightarrow2'$ is equivalent to $3\rightarrow2$ due to symmetry). From site 3′, the V can move to site 4′ with a barrier of 1.53 eV or to site 4″ with a barrier of 1.83 eV. Once the V is in site 4″, it can migrate back to site 1 continuing on the same circular path or following the reverse direction with the same energy barriers for each step. Sites 4, 4′, and 4″ are almost equivalent in energy to the case of completely separate B and V, which means that the V does not feel much effect from the B atom. The results also suggest that if a V in sites 3, 3′, or closer would preferentially migrate toward the substitutional B to form a BV pair, rather than move away from the B site. According to the result, one could also expect V-assisted B diffusion via a ring mechanism in which a V moves around a hexagonal ring to the opposite direction (e.g., $1\rightarrow2\rightarrow3\rightarrow2'\rightarrow1'$); however, the B$V$ pair diffusion tends to be unlikely at moderate temperatures considering the high overall barrier (=4.03 eV).

BV+$V\rightarrow$BV_2. Finally, we looked at how an additional V interacts with the immobile BV pair. As shown in Fig. 7(a), when an additional V meets a BV pair to form a BV_2 complex, it can rearrange into the most stable pentagon-octagon-pentagon (5-8-5) structure, as also predicted for a divacancy [Fig. 7(b)].[19,34] In the configuration, B prefers to be in a site of greater tensile strain because of its larger size compared to C. The energy gain for BV_2 is calculated to be 6.35 eV with respect to (fourfold) BV and single V. Although further Stone-Wales-type rearrangement into another V_2 configuration (consisting of three pentagons and three heptagons), has been predicted to be more energetically favorable than the 5-8-5 configuration, we did not consider the 5-5-5-7-7-7 configuration for BV_2 because of a high-energy barrier for the 5-8-5$\rightarrow$5-5-5-7-7-7 conversion (e.g., ~5.2 eV for V_2).[19] It is now well established that single vacancies can diffuse and coalescence into stable vacancy clusters.[18,19,34,35] Similarly, our study also demonstrates that B-multivacancy clusters can be formed by aggregation of single vacancies, suggesting that substitutional B can possibly act as an anchor for vacancy clusters.

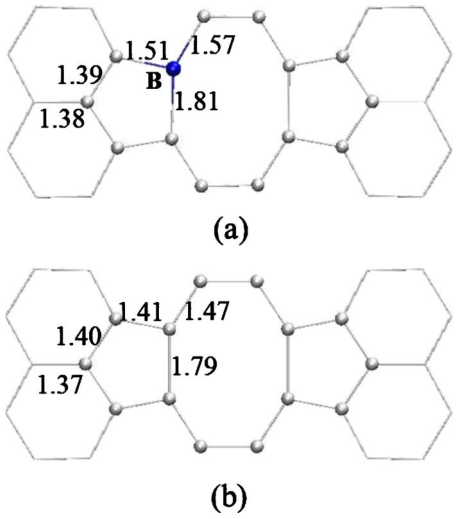

FIG. 7. (Color online) Minimum-energy configurations of (a) BV_2 and (b) V_2. The bond lengths indicated are given in angstrom.

IV. SUMMARY

Based on spin-polarized DFT calculations, we present the formation, structure, and bonding of a BV pair and the effect of BV pairing on the electronic structure of graphene with comparisons to substitutional B and single V. Our calculations show that a mobile V (with a migration barrier of 1.42 eV) can be trapped by substitutional B to form a BV pair with an exothermicity of 2.54 eV. The B in a BV pair energetically prefers to be fourfold coordinated, rather than twofold coordinated, by adopting a tetrahedral configuration with neighboring C atoms but highly distorted due to the rest of the in-plane C lattice. However, the moderate energy difference of 0.33.eV between the fourfold and twofold states may allow their interconversion and consequently magnetic-momentum oscillations; the net magnetic momenta of the twofold and fourfold states are predicted to be about 1 μ_B and 0 μ_B, respectively. Similar to substitutional B, the fourfold BV pair is likely to accept electron, resulting in hole states in graphene. By looking at the migration pathways and energetics of a single V in the vicinity of substitutional B, we find that a vacancy migrating within a few lattice steps of B is likely to migrate closer to the B and becomes trapped. In addition, when an additional V meets a BV pair to form a BV_2 complex, it can undergo rearrangement into the pentagon-octagon-pentagon (5-8-5) geometry; the predicted exothermicity of the $BV+V \rightarrow BV_2$ combination reaction is 6.35 eV. This study suggests that substitutional B would serve as an anchor for vacancy clusters.

ACKNOWLEDGMENTS

This work was supported by the R. A. Welch Foundation (Grant No. F-1535). The authors also thank the Texas Advanced Computing Center for use of their computing resources.

*Author to whom correspondence should be addressed; gshwang@che.utexas.edu

[1] J. Dai, J. Yuan, and P. Giannozzi, Appl. Phys. Lett. **95**, 232105 (2009).
[2] N. Kurita, Carbon **38**, 65 (2000).
[3] M. Endo, C. Kim, T. Karaki, Y. Nishimura, M. J. Matthews, S. D. M. Brown, and M. S. Dresselhaus, Carbon **37**, 561 (1999).
[4] R. H. Miwa, T. B. Martins, and A. Fazzio, Nanotechnology **19**, 155708 (2008).
[5] Y. Ferro, F. Marinelli, A. Jelea, and A. Allouche, J. Chem. Phys. **120**, 11882 (2004).
[6] Z. H. Zhu, G. Q. Lu, and H. Hatori, J. Phys. Chem. B **110**, 1249 (2006).
[7] Y. Zhang, Y. Chen, K. Zhou, C. Liu, J. Zeng, H. Zhang, and Y. Peng, Nanotechnology **20**, 185504 (2009).
[8] M. Sankaran and B. Viswanathan, Carbon **45**, 1628 (2007).
[9] R. Wang, D. Zhang, Y. Zhang, and C. Liu, J. Phys. Chem. B **110**, 18267 (2006).
[10] R. Singh and P. Kroll, J. Phys.: Condens. Matter **21**, 196002 (2009).
[11] L. S. Panchakarla, K. S. Subrahmanyam, S. K. Saha, A. Govindaraj, H. R. Krishnamurthy, U. V. Waghmare, and C. N. R. Rao, Adv. Mater. **21**, 4726 (2009).
[12] M. Endo, T. Hayashi, S. Hong, T. Enoki, and M. S. Dresselhaus, J. Appl. Phys. **90**, 5670 (2001).
[13] C. N. R. Rao, A. K. Sood, R. Voggu, and K. S. Subrahmanyam, J. Phys. Chem. Lett. **1**, 572 (2010).
[14] O. V. Yazyev and L. Helm, Phys. Rev. B **75**, 125408 (2007).
[15] P. O. Lehtinen, A. S. Foster, Y. Ma, A. V. Krasheninnikov, and R. M. Nieminen, Phys. Rev. Lett. **93**, 187202 (2004).
[16] H. Amara, S. Latil, V. Meunier, Ph. Lambin, and J.-C. Charlier, Phys. Rev. B **76**, 115423 (2007).
[17] A. Hashimoto, K. Suenaga, A. Gloter, K. Urita, and S. Iijima, Nature (London) **430**, 870 (2004).
[18] G. D. Lee, C. Z. Wang, E. Yoon, N. M. Hwang, and K. M. Ho, Phys. Rev. B **74**, 245411 (2006).
[19] G. D. Lee, C. Z. Wang, E. Yoon, N. M. Hwang, D. Y. Kim, and K. M. Ho, Phys. Rev. Lett. **95**, 205501 (2005).
[20] I. Suarez-Martinez, A. A. El-Barbary, G. Savini, and M. I. Heggie, Phys. Rev. Lett. **98**, 015501 (2007).
[21] J. P. Perdew and Y. Wang, Phys. Rev. B **45**, 13244 (1992).
[22] G. Kresse and J. Furthmuller, *VASP the Guide* (Vienna University of Technology, Vienna, 2001).
[23] P. E. Blöchl, Phys. Rev. B **50**, 17953 (1994).
[24] H. J. Monkhorst and J. D. Pack, Phys. Rev. B **13**, 5188 (1976).
[25] P. E. Blöchl, O. Jepsen, and O. K. Andersen, Phys. Rev. B **49**, 16223 (1994).
[26] S. H. Vosko, L. Wilk, and M. Nusair, Can. J. Phys. **58**, 1200 (1980).
[27] G. Henkelman, B. P. Uberuaga, and H. Jónsson, J. Chem. Phys. **113**, 9901 (2000).
[28] R. L. Dekock and H. B. Gray, *Chemical Structure and Bonding* (University Science Books, Sausalito, CA, 1989).
[29] S. S. Yu, W. T. Zheng, and Q. Jiang, IEEE Trans. Nanotechnol.

9, 78 (2010).
[30] CPMD, Copyright IBM Corporation 1999–2001, Copyright MPI für Festkörperforschung, Stuttgart, 1997–2004.
[31] E. Kaxiras and K. C. Pandey, Phys. Rev. Lett. **61**, 2693 (1988).
[32] J. Cioslowski and P. Jeffrey Hay, J. Am. Chem. Soc. **112**, 1707 (1990).
[33] A. I. Boldyrev and O. P. Charkin, J. Struct. Chem. **26**, 451 (1985).
[34] M. Saito, K. Yamashita, and T. Oda, Jpn. J. Appl. Phys., Part 2 **46**, L1185 (2007).
[35] Z. Tang, M. Hasegawa, T. Shimamura, Y. Nagai, T. Chiba, Y. Kawazoe, M. Takenaka, E. Kuramoto, and T. Iwata, Phys. Rev. Lett. **82**, 2532 (1999).